PHYSICAL THEORY OF DIFFRACTION EQUIVALENT EDGE CURRENTS FOR TRUNCATED WEDGE STRIPS

Peter M. Johansen

DTIC
SELECTED
DEC 0 8 1995
G

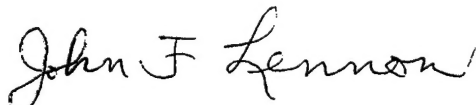*APPROVED FOR PUBLIC RELEASE; DISTRIBUTION UNLIMITED.*

DTIC QUALITY INSPECTED 3

Rome Laboratory
Air Force Materiel Command
Griffiss Air Force Base, New York

This report has been reviewed by the Rome Laboratory Public Affairs Office (PA) and is releasable to the National Technical Information Service (NTIS). At NTIS it will be releasable to the general public, including foreign nations.
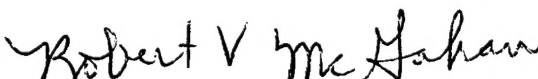
RL-TR-95-217 has been reviewed and is approved for publication.

APPROVED: *John F Lennon*

JOHN F. LENNON
Chief, Applied Electromagnetics Division
Electromagnetics and Reliability Directorate

FOR THE COMMANDER: *Robert V McGahan*

ROBERT V. McGAHAN
Acting Director
Electromagnetics and Reliability Directorate

REPORT DOCUMENTATION PAGE

1. AGENCY USE ONLY (Leave blank)	2. REPORT DATE September 1995	3. REPORT TYPE AND DATES COVERED In-House March-June 1995	

4. TITLE AND SUBTITLE
Physical Theory of Diffraction Equivalent
Edge Currents for Truncated Wedge Strips

5. FUNDING NUMBERS
PE 61102F
PR 2304
TA I4
WU 02

6. AUTHOR(S)

Peter M. Johansen

7. PERFORMING ORGANIZATION NAME(S) AND ADDRESS(ES)
Rome Laboratory/ERCS
31 Grenier St
Hanscom AFB, MA 01731-3010

8. PERFORMING ORGANIZATION REPORT NUMBER

RL-TR-95-217

9. SPONSORING/MONITORING AGENCY NAME(S) AND ADDRESS(ES)

10. SPONSORING/MONITORING AGENCY REPORT NUMBER

11. SUPPLEMENTARY NOTES
Peter M. Johansen, a guest worker from the Electromagnetics Institute,
Technical University of Denmark, completed this work at Rome Laboratory.
Dr. Arthur Yaghjian is the Rome Laboratory POC.

12a. DISTRIBUTION/AVAILABILITY STATEMENT

Approved for public release;
distribution unlimited.

12b. DISTRIBUTION CODE

13. ABSTRACT (Maximum 200 words)

New uniform closed-form expressions for physical theory of diffraction equivalent edge currents are derived for truncated incremental wedge strips. In contrast to previously reported expressions, the new expressions are well-behaved for all directions of incidence and observation and take a finite value for zero strip length. The new expressions are derived by calculating the difference between two terms. The first term is obtained by integrating the exact fringe wave current on a wedge along an un-truncated incremental strip extending from the leading edge of the structure under consideration. The second term is calculated from an integration of the asymptotic fringe wave current along another un-truncated incremental strip extending from the trailing edge of the structure. The new expressions are tested numerically on a triangular cylinder and the results are compared with those obtained using the method of moments and the previously reported expressions.

DTIC QUALITY INSPECTED 3

14. SUBJECT TERMS			15. NUMBER OF PAGES 44
Physical theory of diffraction Equivalent edge currents			**16. PRICE CODE**

17. SECURITY CLASSIFICATION OF REPORT Unclassified	18. SECURITY CLASSIFICATION OF THIS PAGE Unclassified	19. SECURITY CLASSIFICATION OF ABSTRACT Unclassified	20. LIMITATION OF ABSTRACT SAR

Contents

iii

Illustrations

Preface

Chapter 1

Introduction

The physical optics (PO) scattered field from perfectly electrically conducting structures is limited in accuracy because the PO current fails to closely approximate the exact current near surface discontinuities such as edges. The accuracy of the PO scattered field can be significantly increased by adding the fringe wave (FW) field, which takes into account the distortion of the current caused by edges. An approximation to the FW field can be calculated by integrating physical theory of diffraction equivalent edge currents[1],[2] along the illuminated part of the edges of the structure. These edge currents are determined from an integration of the FW current (the exact current minus the PO current) along incremental strips on the canonical wedge or half-plane. Throughout this report only physical theory of diffraction equivalent edge currents will be considered, and these will be referred to as EEC's.

Closed-form expressions for EEC's have been derived for un-truncated (infinite) incremental wedge strips by Michaeli [2], Mitzner [3], and Shore and Yaghjian [4][1]; these EEC's will be called *un-truncated* EEC's in this report. For the analysis of bistatic radar scattering the un-truncated EEC's give an inadequate correction to the PO field due to the presence of the Ufimtsev singularity [2] and the discontinuities of the calculated FW field across the current layers associated with the un-truncated strips. The Ufimtsev singularity occurs when the direction of observation is the continuation of an incident field grazing the face of the structure.

The above-mentioned problems associated with the un-truncated EEC's are eliminated by using truncated (finite) strips. Closed-form expressions for EEC's have been derived for truncated incremental half-plane strips by Breinbjerg [5] and by Shore and Yaghjian [6]. Cote et al. [7] have implicitly derived EEC's for truncated incremental strips on a right-angled

[1]The results by Mitzner [3] and Shore and Yaghjian [4] are expressed in terms of incremental length diffraction coefficients, which are closely related to, and can easily be put in the form of, EEC's.

wedge. Michaeli [8] seems to be the only one who has derived EEC's for general truncated incremental wedge strips; the EEC's based on truncated wedge strips will in this report be called *truncated* EEC's. They apply to the analysis of bistatic radar scattering from three-dimensional structures with flat faces. However, from theoretical considerations, as well as numerical calculations, it appears that Michaeli's truncated EEC's contain non-removable singularities which give rise to numerical problems and thus hamper their application. The singularities are caused by the mathematical procedure applied to obtain closed-form expressions, and they occur for special directions of incidence and observation and for zero strip length.

In this report new truncated EEC's are derived. These EEC's do not have the above-mentioned singularity problems of the previously reported expressions [8], that is, they are well-behaved for all directions of incidence and observation and they take a finite value for zero strip length. The new truncated EEC's are thus well-suited for application to the analysis of bistatic radar scattering from three-dimensional structures with flat faces.

The report is organized as follows. In Chapter 2 the concept of truncated EEC's is introduced. In Chapter 3 it is explained how Michaeli's truncated EEC's are derived and his final expressions are presented. The derivations that lead to the new truncated EEC's are performed in Chapter 4, and finally, Chapter 5 presents numerical examples to illustrate the differences among the fields calculated from the method of moments (applied to the magnetic- and electric field integral equations), the un-truncated EEC's, Michaeli's truncated EEC's, and the new truncated EEC's.

Chapter 2

The Concept of Truncated EEC's

The configuration under consideration is a perfectly conducting three-dimensional structure with flat faces illuminated by a plane wave (see Figure 2.1). In the far field of the structure a high-frequency approximation to the FW field (the total scattered field minus the PO field) is calculated from a line integral along the illuminated part C of the edges of the structure. The truncated EEC's are represented by the magnetic current M_T and the electric current I_T so that the electric FW field is given by [1]

$$\vec{E}^{fw} \sim jk \int_C [ZI_T\hat{s} \times (\hat{s} \times \hat{t}) + M_T\hat{s} \times \hat{t}]\frac{\exp(-jks)}{4\pi s}\, dl \qquad (2.1)$$

where j is the imaginary unit (the time factor $\exp(j\omega t)$ is suppressed), k is the wave number, and Z is the intrinsic impedance of the ambient medium. Furthermore, $\hat{s}$ is the unit vector in the direction of the far-field observation point, s is the distance between the integration and the observation points and $\hat{t}$ is the edge unit tangent vector. The two adjoining faces at each edge are denoted by A and B. It is convenient to introduce a local rectangular xyz-coordinate system with origin at the integration point at the edge. This coordinate system is associated with face A; the unit vector $\hat{x}$ is in the plane of face A, $\hat{y}$ is the outward normal unit vector of this face and $\hat{z}$ equals the edge unit tangent vector $\hat{t}$ (see Figure 2.1). Using this rectangular system, the vector $\hat{s}$ is expressed as $\hat{s} = \hat{x}\sin\beta\cos\phi + \hat{y}\sin\beta\sin\phi + \hat{z}\cos\beta$ where β and ϕ are the polar and azimuthal angles, respectively. The propagation vector $\hat{s}_0$ of the incident plane wave is expressed as $\hat{s}_0 = -\hat{x}\sin\beta_0\cos\phi_0 - \hat{y}\sin\beta_0\sin\phi_0 + \hat{z}\cos\beta_0$ where β_0 and $\phi_0 + \pi$ are the polar and azimuthal angles, respectively (see Figures 2.1 and 2.2). Face B is located in the plane described by $\phi = N\pi$ where $N\pi$ is the exterior wedge angle. Throughout the report it is assumed that $1 < N \leq 2$.

The truncated EEC's are determined by a sum of two contributions, one from each of the faces A and B

$$M_T \;=\; M_T^A + M_T^B \qquad (2.2)$$
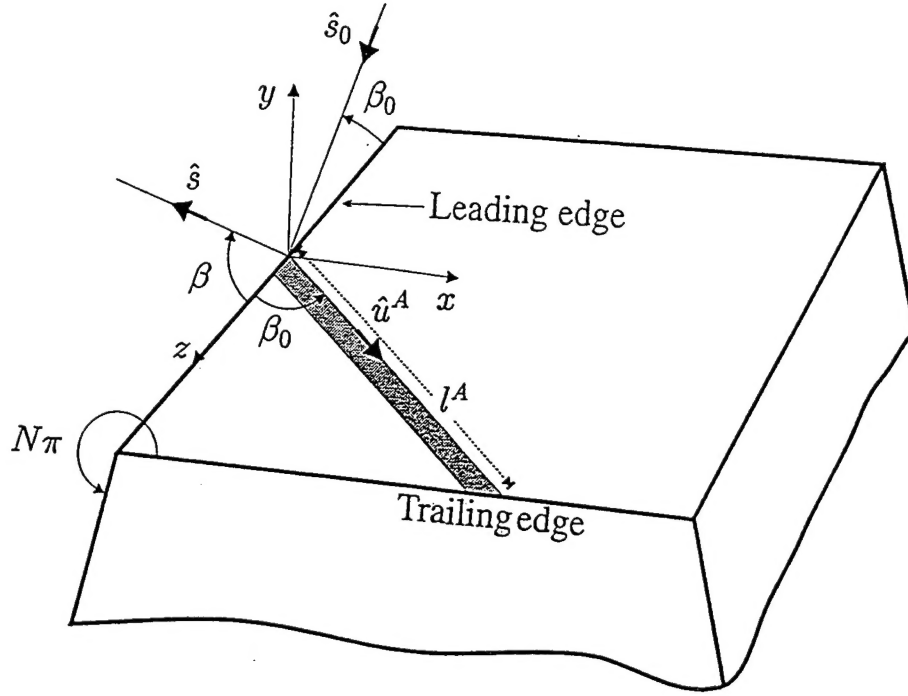
Figure 2.1: Three-dimensional view of a flat face of a three-dimensional structure. The truncated incremental strip extends from the leading edge to the trailing edge and is directed along the unit vector $\hat{u}^A$. The directions of incidence and observation are denoted by $\hat{s}_0$ and $\hat{s}$, respectively. $N\pi$ is the exterior wedge angle and it is assumed that $1 < N \leq 2$.
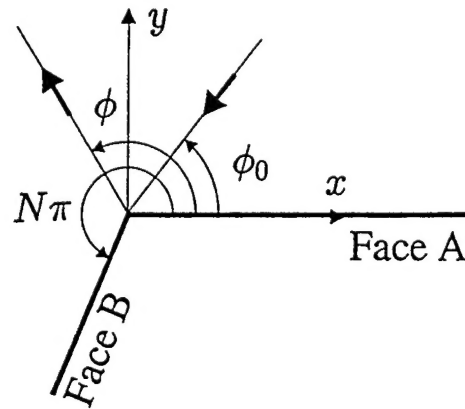
Figure 2.2: Two-dimensional view of the configuration shown in Figure 2.1 in the plane $z = 0$.

$$I_T = I_T^A + I_T^B. \tag{2.3}$$

Henceforth, the superscripts A and B refer to the contributions from the faces A and B, respectively. In this report the contribution from face A will be derived in detail, and the contribution from face B is then obtained from the result for face A using a substitution technique.

The contribution from face A to the truncated EEC's, M_T^A and I_T^A, is calculated analytically by integrating the FW current on face A of a wedge appropriately conforming to the structure along a truncated incremental strip with the length l^A. The strip extends from the *leading edge* (the edge at which the EEC's are placed) to the *trailing edge* and is directed along the unit vector $\hat{u}^A$ which is the intersection of the Keller cone and the face A, as shown in Figure 2.1. However, the integration of the FW current along the truncated incremental strip cannot be performed exactly in closed form and thus, an asymptotic calculation is necessary. To this end, the truncated EEC's are expressed as the difference between the un-truncated EEC's and the *correction* EEC's,

$$M_T = M_{UT} - M_{\text{cor}} \tag{2.4}$$
$$I_T = I_{UT} - I_{\text{cor}}. \tag{2.5}$$

Michaeli [2],[8] found that the un-truncated EEC's can be expressed exactly in closed form whereas closed-form expressions for the correction EEC's can only be obtained using an asymptotic technique. In this report Michaeli's un-truncated EEC's are used but a new asymptotic calculation of the correction EEC's is performed because Michaeli's correction EEC's contain singularities that give rise to numerical problems.

The contribution from face A to the un-truncated EEC's, M_{UT}^A and I_{UT}^A, is obtained by integrating the FW current on face A along an un-truncated incremental strip. The strip extends from the leading edge and is directed along $\hat{u}^A$. Michaeli found that [8, eqs. (3)-(7)]

$$M_{UT}^A = -Z \sin \beta_0 \frac{\sin \phi}{\sin \beta} K_x^A \tag{2.6}$$
$$I_{UT}^A = \sin \beta_0 K_z^A - \sin \beta_0 \cot \beta \cos \phi K_x^A \tag{2.7}$$

with

$$K_{x,z}^A = \int\limits_0^\infty J_{x,z}^{fw,A} \exp(jku\hat{s} \cdot \hat{u}^A) \, du \tag{2.8}$$

where $J_{x,z}^{fw,A}$ denotes the x- and z-components of the FW current on face A.

Similarly, the contribution from face A to the correction EEC's, M_{cor}^A and I_{cor}^A, is obtained by integrating the FW current on face A along another un-truncated incremental strip. This

5

strip extends from the point of truncation at the trailing edge and is directed along $\hat{u}^A$. Thus,

$$M^A_{\text{cor}} = -Z \sin \beta_0 \frac{\sin \phi}{\sin \beta} L^A_x \tag{2.9}$$

$$I^A_{\text{cor}} = \sin \beta_0 L^A_z - \sin \beta_0 \cot \beta \cos \phi L^A_x \tag{2.10}$$

with

$$L^A_{x,z} = \int\limits_{l^A}^{\infty} J^{fw,A}_{x,z} \exp(jku\hat{s} \cdot \hat{u}^A) \, du. \tag{2.11}$$

Michaeli [8] calls the correction EEC's the second-order EEC's but has no designation for the truncated EEC's. In contrast to Michaeli's approach, the correction EEC's in this report are placed at the leading edge instead of the trailing edge.

The truncated EEC's take into account the first-order and part of the second-order edge diffraction. The entire second-order diffraction is not taken into account because the FW current excited at the trailing edge is neglected. It is possible to derive EEC's that take into account the FW current excited at the trailing edge by employing the procedure introduced by Breinbjerg [5]. However, this is not the concern of this report.

Chapter 3

Previous Results

In this chapter the expressions for Michaeli's truncated EEC's are discussed. To understand the approach used for the derivation of the EEC's, the expressions for the exact FW current on face A of the wedge are dealt with first.

3.1 The Exact Fringe Wave Current on Face A of the Wedge

The x- and z-components of the FW current on face A of the wedge can be expressed in terms of a contour integral in the complex ξ-plane [8, eq. (9)] as

$$J_x^{fw,A} = \frac{1}{j\pi N} H_{z0} \exp(-jkz \cos \beta_0) I_1 \tag{3.1}$$

$$J_z^{fw,A} = \frac{j \exp(-jkz \cos \beta_0)}{\pi N} \left(\frac{-E_{z0} \sin \frac{\phi_0}{N}}{Z \sin \beta_0} I_2 + H_{z0} \cot \beta_0 I_3 \right) \tag{3.2}$$

with

$$I_1 = \int_\Gamma \frac{\sin \frac{\xi}{N}}{\cos \frac{\xi}{N} - \cos \frac{\phi_0}{N}} \exp(jX \cos \xi) \, d\xi \tag{3.3}$$

$$I_2 = \int_\Gamma \frac{\sin \xi}{\cos \frac{\xi}{N} - \cos \frac{\phi_0}{N}} \exp(jX \cos \xi) \, d\xi \tag{3.4}$$

$$I_3 = \int_\Gamma \frac{\cos \xi \sin \frac{\xi}{N}}{\cos \frac{\xi}{N} - \cos \frac{\phi_0}{N}} \exp(jX \cos \xi) \, d\xi. \tag{3.5}$$

In these expressions Γ is the steepest descent path through π (see Figure 3.1) and $X = kx \sin \beta_0$. Furthermore, H_{z0} and E_{z0} are the z-components of the incident magnetic and electric field, respectively, at the origin of the local xyz-coordinate system.

7
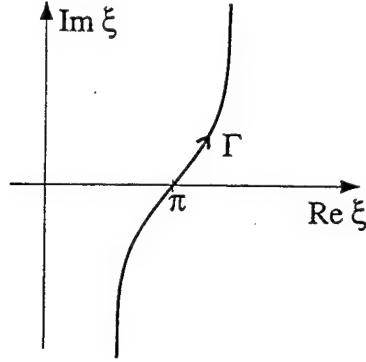
Figure 3.1: The steepest descent path Γ.

The exact FW current given by (3.1) and (3.2) is found in the following way. First, the total field is found for illumination by an electric and magnetic z-directed line source. This is achieved by employing an expansion in terms of eigenfunctions [9, sec. 3.3]. The solution for plane wave TE and TM (with respect to z) incidence is next obtained by moving the line source to infinity. The solution for oblique incidence is obtained by employing the substitution technique described by James [9, p.127] and Bowman et al. [10]. Next, the solution for the total field is expressed in terms of contour integrals and the diffracted field is finally arrived at by deforming the integration contour. Applying the result for the diffracted field, the components (3.1) and (3.2) of the FW current are easily found.

3.2   Un-Truncated EEC's

The calculation of the contribution from face A to the un-truncated EEC's (2.6) and (2.7) is accomplished by insertion of the expressions (3.1) and (3.2) for the exact FW current into the integral $K^A_{x,z}$ in (2.8). Next, the order of integration is interchanged and the inner integral is calculated analytically. Finally, the integration contour Γ is distorted and closed at infinity and thus the integral can be calculated by applying the residue theorem. The results are [2, eqs. (4)-(7)],

$$M^A_{UT} = \frac{2jZH_{z0}\sin\phi}{k\sin\beta_0\sin\beta}\left(\frac{U(\pi-\phi_0)}{\mu+\cos\phi_0} + \frac{\sin\frac{\pi-\alpha}{N}}{N\sin\alpha(\cos\frac{\pi-\alpha}{N} - \cos\frac{\phi_0}{N})}\right) \tag{3.6}$$

and

$$I_{UT}^A = \frac{2j}{kN \sin \beta_0 (\cos \frac{\pi - \alpha}{N} - \cos \frac{\phi_0}{N})} \left(\frac{H_{z0} \sin \frac{\pi - \alpha}{N}}{\sin \alpha} (\cot \beta \cos \phi - \mu \cot \beta_0) - \frac{E_{z0} \sin \frac{\phi_0}{N}}{Z \sin \beta_0} \right)$$
$$+ \frac{2jU(\pi - \phi_0)}{k \sin \beta_0 (\mu + \cos \phi_0)} \left(H_{z0} (\cot \beta \cos \phi + \cot \beta_0 \cos \phi_0) - \frac{E_{z0} \sin \phi_0}{Z \sin \beta_0} \right)$$
$$- \frac{2j \cot \beta_0 H_{z0}}{kN \sin \beta_0} \tag{3.7}$$

where $U(x) = 1$ for $x > 0$ and zero for $x < 0$. Furthermore,

$$\mu = \frac{\sin \beta_0 \sin \beta \cos \phi + \cos \beta_0 (\cos \beta - \cos \beta_0)}{\sin^2 \beta_0} \tag{3.8}$$

and α is the solution to $\mu = \cos \alpha$ determined by

$$\alpha = -j \text{Log}(\mu + \sqrt{\mu^2 - 1}) \tag{3.9}$$

with

$$\text{Log} z = \ln|z| + \text{Arg} z \tag{3.10}$$

and $-\pi < \text{Arg} z \le \pi$. The square root in (3.9) is defined as

$$\sqrt{\mu^2 - 1} = \begin{cases} -|\sqrt{\mu^2 - 1}| & , \quad \mu < -1 \\ j|\sqrt{1 - \mu^2}| & , \quad -1 < \mu < 1. \end{cases} \tag{3.11}$$

The results for M_{UT}^B and I_{UT}^B are obtained from the above expressions by replacing β_0 with $\pi - \beta_0$, β with $\pi - \beta$, ϕ_0 with $N\pi - \phi_0$, and ϕ with $\phi - N\pi$. Using these substitutions it is noted that the last term in (3.7) is canceled by its counterpart in I_{UT}^B.

The singularities of M_{UT}^A and I_{UT}^A have been carefully investigated by Michaeli [2]. The only non-removable singularity is the Ufimtsev singularity [2] which occurs when $\mu = 1$ ($\alpha = 0$) and simultaneously $\phi_0 = \pi$, that is, when the direction of observation is the continuation of an incident field grazing the face of the structure. The Ufimtsev singularity is caused by the lack of phase variation in the integrand of $K_{x,z}^A$ in (2.8) for large values of the integration parameter u and is eliminated by using truncated strips.

3.3 Michaeli's Correction EEC's

The approach used by Michaeli [8] to calculate the contribution from face A to the correction EEC's, M_{cor}^A in (2.9) and I_{cor}^A in (2.10), is as follows. First, the expressions for the exact FW current (3.1) and (3.2) are inserted into the integral $L_{x,z}^A$ in (2.11). Next, the order

9

of integration is interchanged, the inner integral is calculated analytically and finally, the resulting integral is evaluated asymptotically. However, there are two problems associated with this approach. First, the integrand of the resulting integral contains many poles and this fact complicates the task of obtaining an asymptotic expression without non-removable singularities. In fact, Michaeli's asymptotic evaluation results in expressions that contain non-removable singularities for $N \neq 2$. These singularities occur for special directions of incidence and observation. Second, the asymptotic evaluation implies that when $N \neq 2$ the resulting expression has a non-removable singularity for $L = 0$, where $L = kl^A \sin^2 \beta_0$. The above-mentioned singularities give rise to numerical problems and thus hamper the application of the expressions.

To illustrate the above-mentioned problems, Michaeli's asymptotic evaluation of M_{cor}^A is presented below. To distinguish Michaeli's result from the expressions that will be derived in this report, Michaeli's result is denoted by $M_{\text{cor}}^{A'}$.

After the interchange of the order of integration and the analytical calculation of the inner integral, the expression

$$M_{\text{cor}}^{A'} = \frac{ZH_{z0}\sin\phi}{jN\pi k \sin\beta_0 \sin\beta} V \tag{3.12}$$

is arrived at where V is the contour integral

$$V = \int_\Gamma \frac{-j\sin\frac{\xi}{N}\exp(jL(\mu + \cos\xi))}{(\cos\frac{\xi}{N} - \cos\frac{\phi_0}{N})(\mu + \cos\xi)} \, d\xi \tag{3.13}$$

with the contour Γ shown in Figure 3.1. Next, the substitution

$$s = -\sqrt{\frac{2}{j}}\cos\frac{\xi}{2} \tag{3.14}$$

is employed to transform the steepest descent path Γ to the real s-axis whereby the integral V in (3.13) becomes

$$V = \sqrt{\frac{2}{j}}\exp(jL(\mu - 1))\int_{-\infty}^{\infty} W(\xi)\exp(-Ls^2) \, ds \tag{3.15}$$

where $\sqrt{j}$ means $\exp(j\frac{\pi}{4})$ and

$$W(\xi) = \frac{\sin\frac{\xi}{N}}{\sin\frac{\xi}{2}(\cos\frac{\xi}{N} - \cos\frac{\phi_0}{N})(\mu + \cos\xi)}. \tag{3.16}$$

To isolate the singularities of $W(\xi)$ close to the saddle point $\xi = \pi$ ($s = 0$), Michaeli applied a decomposition of the form

$$W(\xi) = \frac{C}{s + \frac{a}{\sqrt{j}}} + \frac{Ds + E}{s^2 + jb^2} + S(\xi) \tag{3.17}$$

10

with the assumption that $S(\xi)$ is a regular function,

$$S(\xi) = W(\xi) - \frac{C}{s + \frac{a}{\sqrt{j}}} - \frac{Ds + E}{s^2 + jb^2}. \tag{3.18}$$

In the expression (3.17) for $W(\xi)$, $a = \sqrt{2}\cos\frac{\phi_0}{2}$ and $b = \sqrt{2}\sin\frac{\alpha}{2}$. The first term on the right side of (3.17) takes into account the pole of $(\cos\frac{\xi}{N} - \cos\frac{\phi_0}{N})^{-1}$ near the saddle point $(\xi = \pi)$ when $\phi_0 = \pi$. The second term on the right side of (3.17) takes into account the two poles of $(\mu + \cos\xi)^{-1}$ near the saddle point when $\alpha = 0$ (recall that $\mu = \cos\alpha$). There is a problem associated with the decomposition (3.17). The problem occurs when the decomposition constant E is to be determined[1]. To calculate this constant one multiplies equation (3.17) by $s^2 + jb^2$ on both sides. It is seen that $\mu + \cos\xi \to 0$ and $s^2 + jb^2 \to 0$ for $\xi \to \pi \pm \alpha$. Thus, by employing the fact that $S(\xi)$ is regular and by calculating the limits for $\xi \to \pi - \alpha$ and $\xi \to \pi + \alpha$, and combining the two results, the constant E is determined. However, if $N \neq 2$ and $\alpha = \pi$ the quantity $\sin\frac{\xi}{N}(\sin\frac{\xi}{2})^{-1}$ appearing in (3.16) tends to infinity for $\xi \to \pi + \alpha$ and this singularity is not accounted for by the decomposition (3.17). Since $S(\xi)$ is assumed regular the singularity for $\alpha = \pi$ will appear in the decomposition constant E. For $N = 2$ the quantity $\sin\frac{\xi}{N}(\sin\frac{\xi}{2})^{-1}$ equals 1, and no problem occurs. Further, for $\phi_0 = -(\pi + \alpha) + 2\pi N$ the quantity $(\cos\frac{\xi}{N} - \cos\frac{\phi_0}{N})^{-1}$, which appears in the expression (3.16) for $W(\xi)$, goes to infinity for $\xi \to \pi + \alpha$. If $N = 2$ this singularity will be accounted for by the term $C(s + \frac{a}{\sqrt{j}})^{-1}$ in (3.17). If, on the other hand, $N \neq 2$ there will be no term on the right side of (3.17) that will take this singularity into account and thus, the singularity appears in E. In summary, the decomposition constant E contains two singularities when $N \neq 2$. These occur for $\alpha = \pi$ and for $\phi_0 = -(\pi + \alpha) + 2\pi N$.

The first two terms on the right side of (3.17) are integrated explicitly using (3.15) and expressed in terms of Fresnel functions. The third term of (3.17) is integrated asymptotically for $L \gg 1$ using the standard steepest descent technique [11]. For $N \neq 2$ this technique implies that the resulting expression tends to infinity for $L \to 0$. This can occur for edge points close to corners in the evaluation of the integral (2.1). As discussed by Michaeli [8] it is possible to avoid small values of L by omitting part of the edge which is close to corners in the evaluation of the integral (2.1). However, this approach is not satisfactory since the calculated field will depend on the ratio of the edge being omitted. For $N = 2$ the asymptotic calculation equals the exact solution and thus, no singularity occurs when $L = 0$.

To summarize, the singularities occurring for $\phi_0 = -(\pi + \alpha) + 2\pi N$ and $\alpha = \pi$ are caused by the decomposition of the integrand (3.16) that contains many poles. It is noted that the quantity $\mu + \cos\xi$ in the denominator of (3.16) is caused by the analytical calculation of the inner integral after the order of integration is interchanged (see the summary of

---

[1] It is not necessary to determine the constant D because the odd term $\frac{Ds}{s^2+jb^2}$ vanishes when integrated from $-\infty$ to ∞, see (3.15).

Michaeli's approach at the beginning of this section). Thus, the interchange of the order of integration and the following analytical calculation of the inner integral introduce more poles to the integrand. Furthermore, the singularity for $L = 0$ is caused by the use of the standard steepest descent technique on the integral (3.15) containing the exponential factor $\exp(-Ls^2)$. This exponential factor is introduced by the analytical calculation of the inner integral. It is therefore seen that the singularity problems of Michaeli's expressions are basically caused by the interchange of the order of integration when the integral $L^A_{x,z}$ in (2.11) is calculated. In the following chapter the integral $L^A_{x,z}$ will be calculated without interchanging the order of integration. By this approach the singularity problems described in this section are avoided.

The asymptotic results for $M^{A'}_{\text{cor}}$ and $I^{A'}_{\text{cor}}$, valid for $L \gg 1$, are [8]

$$
\begin{aligned}
M^{A'}_{\text{cor}} = \ & \frac{Z H_{z0} \sin\phi \exp(jL(\mu - 1))}{j\pi N k \sin\beta_0 \sin\beta} \left[\frac{-2\pi N \mathrm{sgn}(\cos\frac{\phi_0}{2})}{\mu + \cos\phi_0} K(\sqrt{2L}|\cos\frac{\phi_0}{2}|) \right. \\
& - \frac{2\pi}{\sin\alpha} \left(\frac{\sin\frac{\pi-\alpha}{N}}{\cos\frac{\pi-\alpha}{N} - \cos\frac{\phi_0}{N}} + \frac{\sin\frac{\pi+\alpha}{N}}{\cos\frac{\pi+\alpha}{N} - \cos\frac{\phi_0}{N}} \right) K(\sqrt{L(1-\mu)}) \\
& \left. + \sqrt{\frac{2\pi}{jL}} \frac{\sin\frac{\pi}{N}}{(\cos\frac{\pi}{N} - \cos\frac{\phi_0}{N})(\mu - 1)} \right]
\end{aligned}
\tag{3.19}
$$

$$
\begin{aligned}
I^{A'}_{\text{cor}} = \ & \frac{2\exp(jL(\mu - 1))}{jkN\sin\beta_0} \left\{ \frac{N\mathrm{sgn}(\cos\frac{\phi_0}{2})}{\mu + \cos\phi_0} \right. \\
& \cdot \left(-H_{z0}(\cot\beta\cos\phi + \cot\beta_0\cos\phi_0) + \frac{E_{z0}\sin\phi_0}{Z\sin\beta_0} \right) K(\sqrt{2L}|\cos\frac{\phi_0}{2}|) \\
& + \left[\frac{H_{z0}}{\sin\alpha} \left(\frac{\sin\frac{\pi-\alpha}{N}}{\cos\frac{\pi-\alpha}{N} - \cos\frac{\phi_0}{N}} + \frac{\sin\frac{\pi+\alpha}{N}}{\cos\frac{\pi+\alpha}{N} - \cos\frac{\phi_0}{N}} \right) (\mu\cot\beta_0 - \cot\beta\cos\phi) \right. \\
& + \frac{E_{z0}\sin\frac{\phi_0}{N}}{Z\sin\beta_0} \left. \left(\frac{1}{\cos\frac{\pi-\alpha}{N} - \cos\frac{\phi_0}{N}} - \frac{1}{\cos\frac{\pi+\alpha}{N} - \cos\frac{\phi_0}{N}} \right) \right] K(\sqrt{L(1-\mu)}) \\
& \left. + \frac{H_{z0}\sin\frac{\pi}{N}(\cot\beta\cos\phi - \cot\beta_0)}{\sqrt{2\pi jL}(\cos\frac{\pi}{N} - \cos\frac{\phi_0}{N})(\mu - 1)} \right\}.
\end{aligned}
\tag{3.20}
$$

In these expressions $\mathrm{sgn}(a) = \frac{|a|}{a}$ and

$$
K(x) = F(x) - \frac{1}{2\sqrt{j\pi}x}
\tag{3.21}
$$

where F is a modified Fresnel function

$$
F(x) = \sqrt{\frac{j}{\pi}} \exp(jx^2) \int_x^\infty \exp(-jt^2)\, dt.
\tag{3.22}
$$

12

It is noted that the expressions for $M_{\text{cor}}^{A'}$ and $I_{\text{cor}}^{A'}$ contain non-removable singularities when $N \neq 2$. These singularities occur for $L = 0$, $\alpha = \pi$, and $\phi_0 = -(\pi + \alpha) + 2\pi N$.

The expressions for $M_{\text{cor}}^{B'}$ and $I_{\text{cor}}^{B'}$ are obtained by applying the substitutions listed after equation (3.11). Furthermore, the strip length on face A, l^A, must be replaced by the strip length on face B, l^B.

Chapter 4

Derivation of New Correction EEC's

As summarized in Section 3.3 the singularity problems associated with Michaeli's correction EEC's are caused by the interchange of the order of integration when calculating the integral $L_{x,z}^A$ in (2.11). In this chapter another approach is used to calculate $L_{x,z}^A$. Instead of applying the exact expressions for the FW current in the integral $L_{x,z}^A$, the asymptotic expressions for the FW current are employed. Thus, the first section in this chapter deals with the determination of the asymptotic expressions for the FW current.

4.1 Uniform Asymptotic Expressions for the Fringe Wave Current on Face A

To obtain a uniform asymptotic expression for the FW current, the steepest descent technique [11] is applied to the integrals $I_1, I_2,$ and I_3 given by (3.3)–(3.5). The steepest descent path Γ is first transformed to the real s-axis using the substitution (3.14)

$$s = -\sqrt{\frac{2}{j}} \cos\frac{\xi}{2} \tag{4.1}$$

where $\sqrt{j}$ means $\exp(j\frac{\pi}{4})$. For I_1 this yields

$$I_1 = \sqrt{2j}\exp(-jX)\int\limits_{-\infty}^{\infty} T(\xi)\exp(-Xs^2)\,ds \tag{4.2}$$

where

$$T(\xi) = \frac{\sin\frac{\xi}{N}}{\sin\frac{\xi}{2}(\cos\frac{\xi}{N} - \cos\frac{\phi_0}{N})}. \tag{4.3}$$

To isolate the pole of the integrand near the saddle point ($\xi = \pi$) a decomposition technique similar to the one applied by Michaeli [8, eq. (29)] is used. Thus, $T(\xi)$ in (4.3) is written as a sum of a simple pole term and a regular term,

$$T(\xi) = \frac{A}{s + \frac{a}{\sqrt{j}}} + R(\xi) \tag{4.4}$$

where $a = \sqrt{2}\cos\frac{\phi_0}{2}$ and the regular term is

$$R(\xi) = T(\xi) - \frac{A}{s + \frac{a}{\sqrt{j}}}. \tag{4.5}$$

The poles of the first term on the right side of (4.4) are determined by $\xi = \pm\phi_0 + 4\pi n$, n being an integer, and thus, the pole at $\xi = \pi$ is isolated for $\phi_0 = \pi$. The decomposition (4.4) contains only one simple pole term and is thus simpler than the decomposition presented in Section 3.3. Due to the simpler decomposition, the singularity problems encountered in Section 3.3 will not appear.

The decomposition constant A is determined from

$$A = \lim_{\xi \to \phi_0} \frac{\sqrt{\frac{2}{j}}\sin\frac{\xi}{N}(-\cos\frac{\xi}{2} + \cos\frac{\phi_0}{2})}{\sin\frac{\xi}{2}(\cos\frac{\xi}{N} - \cos\frac{\phi_0}{N})} = \frac{-N}{\sqrt{2j}}. \tag{4.6}$$

The integration of the first term on the right side of (4.4) is written as

$$\int_{-\infty}^{\infty} \frac{\exp(-Xs^2)}{s + \frac{a}{\sqrt{j}}}\,ds = \frac{-a}{\sqrt{j}}\int_{-\infty}^{\infty} \frac{\exp(-Xs^2)}{s^2 - \frac{a^2}{j}}\,ds. \tag{4.7}$$

The integral on the right side of (4.7) is then evaluated using [12, eq. (12)] and expressed in terms of the modified Fresnel function (3.22)

$$F(x) = \sqrt{\frac{j}{\pi}}\exp(jx^2)\int_{x}^{\infty} \exp(-jt^2)\,dt \tag{4.8}$$

with the result

$$\int_{-\infty}^{\infty} \frac{\exp(-Xs^2)}{s + \frac{a}{\sqrt{j}}}\,ds = 2j\pi\,\text{sgn}(a)F(|a|\sqrt{X}) \tag{4.9}$$

where $\text{sgn}(a) = \frac{|a|}{a}$. Since the function $R(\xi)$ is regular near the saddle point, the standard steepest descent technique is applied to the second term on the right side of (4.4),

$$\int_{-\infty}^{\infty} R(\xi)\exp(-Xs^2)\,ds \sim R(\pi)\sqrt{\frac{\pi}{X}} \qquad \text{for} \quad X \gg 1. \tag{4.10}$$

15

Thus, the asymptotic expression for I_1 is

$$I_1 \sim -2j\pi N \exp(-jX)\mathrm{sgn}(a)F(|a|\sqrt{X})$$
$$+\sqrt{\frac{2j\pi}{X}}\exp(-jX)\left(\frac{\sin\frac{\pi}{N}}{\cos\frac{\pi}{N}-\cos\frac{\phi_0}{N}}+\frac{N}{\sqrt{2}a}\right). \tag{4.11}$$

The same procedure is used to calculate the asymptotic expressions for I_2 and I_3. The results are (see Appendix A)

$$I_2 \sim \frac{-2jN\pi\sin\phi_0\exp(-jX)}{\sin\frac{\phi_0}{N}}\mathrm{sgn}(a)\left(F(|a|\sqrt{X})-\frac{1}{2\sqrt{j\pi X}|a|}\right) \tag{4.12}$$

$$I_3 \sim -2j\pi N\mathrm{sgn}(a)\cos\phi_0\exp(-jX)F(|a|\sqrt{X})$$
$$+\sqrt{\frac{2j\pi}{X}}\exp(-jX)\left(\frac{N\cos\phi_0}{\sqrt{2}a}-\frac{\sin\frac{\pi}{N}}{\cos\frac{\pi}{N}-\cos\frac{\phi_0}{N}}\right). \tag{4.13}$$

The asymptotic expressions for $J_x^{fw,A}$ in (3.1) and $J_z^{fw,A}$ in (3.2), valid for $X=kx\sin\beta_0\gg 1$, are obtained by employing the above results for I_1, I_2, and I_3,

$$J_x^{fw,A} \sim -2H_{z0}\exp(-jk\hat{u}^A\cdot\vec{r})\left[\mathrm{sgn}(\cos\frac{\phi_0}{2})F(\sqrt{2kx\sin\beta_0}|\cos\frac{\phi_0}{2}|)\right.$$
$$\left.-\frac{1}{\sqrt{2j\pi kx\sin\beta_0}}\left(\frac{1}{2\cos\frac{\phi_0}{2}}+\frac{\sin\frac{\pi}{N}}{N(\cos\frac{\pi}{N}-\cos\frac{\phi_0}{N})}\right)\right] \tag{4.14}$$

and

$$J_z^{fw,A} \sim -2\exp(-jk\hat{u}^A\cdot\vec{r})\left[\left(\frac{E_{z0}\sin\phi_0}{Z\sin\beta_0}-H_{z0}\cot\beta_0\cos\phi_0\right)\right.$$
$$\cdot\mathrm{sgn}(\cos\frac{\phi_0}{2})F(\sqrt{2kx\sin\beta_0}|\cos\frac{\phi_0}{2}|)$$
$$-\frac{E_{z0}\sin\phi_0}{Z\sin\beta_0 2\sqrt{2j\pi kx\sin\beta_0}\cos\frac{\phi_0}{2}}$$
$$\left.+\frac{H_{z0}\cot\beta_0}{\sqrt{2j\pi kx\sin\beta_0}}\left(\frac{\cos\phi_0}{2\cos\frac{\phi_0}{2}}-\frac{\sin\frac{\pi}{N}}{N(\cos\frac{\pi}{N}-\cos\frac{\phi_0}{N})}\right)\right] \tag{4.15}$$

where $\vec{r}=\hat{x}x+\hat{z}z$ and $\hat{u}^A=\hat{x}\sin\beta_0+\hat{z}\cos\beta_0$. The formulas for the FW current can also be expressed in terms of the function $K(x)$ in (3.21),

$$K(x)=F(x)-\frac{1}{2\sqrt{j\pi x}} \tag{4.16}$$

16

where $K(x) \approx 0$ for $x > 3$. One finds

$$J_x^{fw,A} \sim -2H_{z0}\exp(-jk\hat{u}^A \cdot \vec{r})\left(\text{sgn}(\cos\frac{\phi_0}{2})K(\sqrt{2kx\sin\beta_0}|\cos\frac{\phi_0}{2}|)\right.$$
$$\left. -\frac{\sin\frac{\pi}{N}}{N\sqrt{2j\pi kx\sin\beta_0}(\cos\frac{\pi}{N} - \cos\frac{\phi_0}{N})}\right) \tag{4.17}$$

$$J_z^{fw,A} \sim -2\exp(-jk\hat{u}^A \cdot \vec{r})\left[\left(\frac{E_{z0}\sin\phi_0}{Z\sin\beta_0} - H_{z0}\cot\beta_0\cos\phi_0\right)\right.$$
$$\cdot\text{sgn}(\cos\frac{\phi_0}{2})K(\sqrt{2kx\sin\beta_0}|\cos\frac{\phi_0}{2}|)$$
$$\left. -\frac{H_{z0}\cot\beta_0\sin\frac{\pi}{N}}{N\sqrt{2j\pi kx\sin\beta_0}(\cos\frac{\pi}{N} - \cos\frac{\phi_0}{N})}\right]. \tag{4.18}$$

The representations (4.14) and (4.15) are well-suited for the analytical calculation of the FW current in the limit $\phi_0 \to \pi$, whereas using the equations (4.17) and (4.18) is more convenient to obtain expressions for the FW current when $\sqrt{2kx\sin\beta_0}|\cos\frac{\phi_0}{2}| > 3$.

4.2 Calculation of the Integrals L_x^A and L_z^A

To derive the results for M_{cor}^A in (2.9) and I_{cor}^A in (2.10), the expressions for L_x^A and L_z^A given in (2.11) are needed. First, L_x^A is calculated. To this end the x-component of the asymptotic FW current (4.14) is inserted into the integral L_x^A. The integration variable u of $L_{x,z}^A$ is the distance along the Keller cone and thus the substitutions $x = u\sin\beta_0$ and $z = u\cos\beta_0$ are applied. Since the asymptotic expression for the FW current applies for $ku\sin^2\beta_0 \gg 1$ the asymptotic result for L_x^A applies for $L = kl^A\sin^2\beta_0 \gg 1$,

$$L_x^A = \int_{l^A}^{\infty} J_x^{A,fw}\exp(jku\hat{s}\cdot\hat{u}^A)\,du$$

$$\sim -2H_{z0}\text{sgn}(\cos\frac{\phi_0}{2})\int_{l^A}^{\infty} F(\sqrt{2ku}\sin\beta_0|\cos\frac{\phi_0}{2}|)\exp(-jku\sin^2\beta_0(1-\mu))\,du$$

$$+\frac{2H_{z0}}{\sqrt{2j\pi k}\sin\beta_0}\left(\frac{1}{2\cos\frac{\phi_0}{2}} + \frac{\sin\frac{\pi}{N}}{N(\cos\frac{\pi}{N} - \cos\frac{\phi_0}{N})}\right)\int_{l^A}^{\infty}\frac{\exp(-jku\sin^2\beta_0(1-\mu))}{\sqrt{u}}\,du \tag{4.19}$$

17

where the identity $1 - \hat{s} \cdot \hat{u}^A = \sin^2 \beta_0 (1 - \mu)$, with μ defined in (3.8), has been applied. The two integrals in (4.19) are evaluated in Appendix B. Hence,

$$
\begin{aligned}
L_x^A \sim \; & \frac{2 \exp(jL(\mu - 1)) H_{z0}}{jk \sin^2 \beta_0} \left[\frac{\operatorname{sgn}(\cos \frac{\phi_0}{2})}{\mu + \cos \phi_0} \left(F(\sqrt{2L} | \cos \frac{\phi_0}{2} |) \right. \right. \\
& \left. - \frac{\sqrt{2} | \cos \frac{\phi_0}{2} |}{\sqrt{1 - \mu}} F(\sqrt{L(1 - \mu)}) \right) \\
& \left. + \frac{\sqrt{2}}{\sqrt{1 - \mu}} \left(\frac{1}{2 \cos \frac{\phi_0}{2}} + \frac{\sin \frac{\pi}{N}}{N(\cos \frac{\pi}{N} - \cos \frac{\phi_0}{N})} \right) F(\sqrt{L(1 - \mu)}) \right].
\end{aligned}
\tag{4.20}
$$

Second, L_z^A is calculated. The asymptotic expression for the z-component of the FW current (4.15) is inserted into the integral L_z^A in (2.11) to yield

$$
\begin{aligned}
L_z^A = \; & \int_{l^A}^{\infty} J_z^{A, fw} \exp(jku\hat{s} \cdot \hat{u}^A) \, du \\
\sim \; & -2 \left(\frac{E_{z0} \sin \phi_0}{Z \sin \beta_0} - H_{z0} \cot \beta_0 \cos \phi_0 \right) \operatorname{sgn}(\cos \frac{\phi_0}{2}) \\
& \cdot \int_{l^A}^{\infty} F(\sqrt{2ku} \sin \beta_0 | \cos \frac{\phi_0}{2} |) \exp(-jku \sin^2 \beta_0 (1 - \mu)) \, du \\
& + \left[\left(\frac{E_{z0} \sin \phi_0}{Z \sin \beta_0} - H_{z0} \cot \beta_0 \cos \phi_0 \right) \frac{1}{\sqrt{2j\pi k} \sin \beta_0 \cos \frac{\phi_0}{2}} \right. \\
& \left. + \frac{2 H_{z0} \cot \beta_0 \sin \frac{\pi}{N}}{N \sqrt{2j\pi k} \sin \beta_0 (\cos \frac{\pi}{N} - \cos \frac{\phi_0}{N})} \right] \\
& \cdot \int_{l^A}^{\infty} \frac{\exp(-jku \sin^2 \beta_0 (1 - \mu))}{\sqrt{u}} \, du.
\end{aligned}
\tag{4.21}
$$

When the results of Appendix B are applied, L_z^A is expressed as

$$
\begin{aligned}
L_z^A \sim \; & \frac{2 \exp(jL(\mu - 1))}{jk \sin^2 \beta_0} \left\{ \left(\frac{E_{z0} \sin \phi_0}{Z \sin \beta_0} - H_{z0} \cot \beta_0 \cos \phi_0 \right) \frac{\operatorname{sgn}(\cos \frac{\phi_0}{2})}{\mu + \cos \phi_0} F(\sqrt{2L} | \cos \frac{\phi_0}{2} |) \right. \\
& + \left[H_{z0} \cot \beta_0 \left(\frac{\cos \frac{\phi_0}{2} \cos \phi_0}{\mu + \cos \phi_0} - \frac{\cos \phi_0}{2 \cos \frac{\phi_0}{2}} + \frac{\sin \frac{\pi}{N}}{N(\cos \frac{\pi}{N} - \cos \frac{\phi_0}{N})} \right) \right. \\
& \left. \left. + \frac{E_{z0} \sin \frac{\phi_0}{2} (\mu - 1)}{Z \sin \beta_0 (\mu + \cos \phi_0)} \right] \frac{\sqrt{2} F(\sqrt{L(1 - \mu)})}{\sqrt{1 - \mu}} \right\}.
\end{aligned}
\tag{4.22}
$$

18

4.3 Expressions for the Correction EEC's

The asymptotic expressions for the contribution from face A to the correction EEC's, M_{cor}^A in (2.9) and I_{cor}^A in (2.10), are now obtained by employing the results for L_x^A in (4.20) and L_z^A in (4.22),

$$
M_{cor}^A \sim \frac{2 Z H_{z0} \sin \phi \exp(jL(\mu - 1))}{jk \sin \beta \sin \beta_0} \left[\frac{-\mathrm{sgn}(\cos \frac{\phi_0}{2})}{\mu + \cos \phi_0} F(\sqrt{2L}|\cos \frac{\phi_0}{2}|) \right.
$$
$$
\left. + \left(\frac{\sqrt{1 - \mu}}{\sqrt{2}(\mu + \cos \phi_0) \cos \frac{\phi_0}{2}} - \frac{\sqrt{2} \sin \frac{\pi}{N}}{N\sqrt{1 - \mu}(\cos \frac{\pi}{N} - \cos \frac{\phi_0}{N})} \right) F(\sqrt{L(1 - \mu)}) \right]
$$
(4.23)

$$
I_{cor}^A \sim \frac{2 \exp(jL(\mu - 1))}{jk \sin \beta_0(\mu + \cos \phi_0)} \left[\mathrm{sgn}(\cos \frac{\phi_0}{2}) F(\sqrt{2L}|\cos \frac{\phi_0}{2}|) \right.
$$
$$
\cdot \left(\frac{E_{z0} \sin \phi_0}{Z \sin \beta_0} - H_{z0}(\cot \beta_0 \cos \phi_0 + \cot \beta \cos \phi) \right)
$$
$$
+ \sqrt{2(1 - \mu)} F(\sqrt{L(1 - \mu)}) \left(-\frac{E_{z0} \sin \frac{\phi_0}{2}}{Z \sin \beta_0} + \frac{H_{z0}}{2 \cos \frac{\phi_0}{2}}(\cot \beta_0 \cos \phi_0 + \cot \beta \cos \phi) \right.
$$
$$
\left. \left. + \frac{H_{z0} \sin \frac{\pi}{N}(\mu + \cos \phi_0)(\cot \beta_0 - \cot \beta \cos \phi)}{N(\cos \frac{\pi}{N} - \cos \frac{\phi_0}{N})(1 - \mu)} \right) \right].
$$
(4.24)

The final expressions for the truncated EEC's are obtained by first calculating M_T^A and I_T^A by subtracting the above results, (4.23) and (4.24), from the un-truncated EEC's, (3.6) and (3.7), as shown in (2.4) and (2.5). Second, the contribution from face B is calculated using the results for M_T^A and I_T^A by replacing β_0 with $\pi - \beta_0$, β with $\pi - \beta$, ϕ_0 with $N\pi - \phi_0$, ϕ with $N\pi - \phi$, and l^A with l^B. Third, the contributions from the two faces are added in order to determine M_T and I_T, see (2.2) and (2.3). Finally, these expressions are inserted into the radiation integral (2.1) to determine the approximate FW field from the truncated EEC's.

It is noted that M_{cor}^A in (4.23) and I_{cor}^A in (4.24) do not contain singularities for $\alpha = \pi$ ($\mu = -1$), $\phi_0 = -(\pi + \alpha) + 2\pi N$, and $L = 0$ as do the previously reported expressions (3.19) and (3.20). Using the result of [2, app. II] it is shown that when $\phi_0 \neq \pi$ the quantities $\sin \phi (1 - \mu)^{-\frac{1}{2}}$ and $(\cot \beta_0 - \cot \beta \cos \phi)(1 - \mu)^{-\frac{1}{2}}$, which appear in the expressions for M_{cor}^A in (4.23) and I_{cor}^A in (4.24), remain bounded for $\mu \to 1$. If $\phi_0 = \pi$ and $\mu \to 1$, M_{cor}^A and I_{cor}^A are singular but this singularity (the Ufimtsev singularity) is canceled by the singularity in M_{UT}^A and I_{UT}^A given by (3.6) and (3.7), respectively. This means that M_T and I_T are valid for all directions of incidence and observation. Besides, the fact that M_{cor}^A and I_{cor}^A are finite for $L = 0$ implies that no numerical problems arise when the strip length becomes small. This can occur for edge points close to corners of the structure. However, the field calculated

from the truncated EEC's for these edge points is a poor approximation to the exact field for two reasons: First, the asymptotic expressions for the correction EEC's are invalid and second, the distortion of the current on the structure near corners is not taken into account.

4.4   Special Cases

If it is assumed that the arguments $\sqrt{2L}|\cos\frac{\phi_0}{2}|$ and $\sqrt{L(1-\mu)}$ of the modified Fresnel functions in (4.23) and (4.24) are so large that the asymptotic formula [8, eq. (40)]

$$F(x) \sim \frac{1}{2x\sqrt{j\pi}} \tag{4.25}$$

can be applied, M_{cor}^A in (4.23) and I_{cor}^A in (4.24) become

$$M_{\text{cor}}^A \sim \frac{-\sqrt{2}ZH_{z0}\sin\phi\sin\frac{\pi}{N}\exp(jL(\mu-1))}{jk\sin\beta\sin\beta_0\sqrt{j\pi LN}(1-\mu)(\cos\frac{\pi}{N}-\cos\frac{\phi_0}{N})} \tag{4.26}$$

$$I_{\text{cor}}^A \sim \frac{\sqrt{2}H_{z0}\sin\frac{\pi}{N}(\cot\beta_0-\cot\beta\cos\phi)\exp(jL(\mu-1))}{jk\sin\beta_0\sqrt{j\pi LN}(1-\mu)(\cos\frac{\pi}{N}-\cos\frac{\phi_0}{N})}. \tag{4.27}$$

Except for $\phi_0 = -(\pi + \alpha) + 2\pi N$ and $\alpha = \pi$ ($\mu = -1$) these expressions are the same as those obtained using Michaeli's correction EEC's [8].

For the half-plane, that is, $N = 2$, the expressions for M_{cor}^A in (4.23) and I_{cor}^A in (4.24) simplify. Besides, the uniform asymptotic FW current found in Section 4.1 equals the exact FW current. This means that M_{cor}^A in (4.23) and I_{cor}^A in (4.24) are valid for any value of L. The correction EEC's, that is, the sum of the contributions from faces A and B, become

$$M_{\text{cor}} = \frac{4ZH_{z0}\sin\phi\exp(jL(\mu-1))}{jk\sin\beta\sin\beta_0(\mu+\cos\phi_0)}\left(-\text{sgn}(\cos\frac{\phi_0}{2})F(\sqrt{2L}|\cos\frac{\phi_0}{2}|)\right.$$
$$\left.+\frac{\sqrt{2}\cos\frac{\phi_0}{2}}{\sqrt{1-\mu}}F(\sqrt{L(1-\mu)})\right) \tag{4.28}$$

20

and

$$I_{\text{cor}} = \frac{4E_{z0}\sin\frac{\phi_0}{2}\exp(jL(\mu-1))}{jkZ\sin^2\beta_0(\mu+\cos\phi_0)}\left(2|\cos\frac{\phi_0}{2}|F(\sqrt{2L}|\cos\frac{\phi_0}{2}|)\right.$$
$$\left.-\sqrt{2(1-\mu)}F(\sqrt{L(1-\mu)})\right)$$
$$+\frac{4H_{z0}\exp(jL(\mu-1))}{jk\sin\beta_0(\mu+\cos\phi_0)}\left(-\text{sgn}(\cos\frac{\phi_0}{2})\right.$$
$$\cdot(\cot\beta_0\cos\phi_0+\cot\beta\cos\phi)F(\sqrt{2L}|\cos\frac{\phi_0}{2}|)$$
$$\left.+\frac{\sqrt{2}\cos\frac{\phi_0}{2}(\cot\beta\cos\phi-\mu\cot\beta_0)}{\sqrt{1-\mu}}F(\sqrt{L(1-\mu)})\right) \tag{4.29}$$

which are the same results obtained using Michaeli's expressions [8]. The expressions (4.28) and (4.29) are further verified by letting $l^A = 0$. In this case $M_{\text{cor}} = M_{UT}$ and $I_{\text{cor}} = I_{UT}$. Thus, the truncated EEC's, M_T in (2.4) and I_T in (2.5), are zero which is the result obtained by integrating the FW current along a strip with length zero.

Chapter 5

Numerical Results

In this chapter the field scattered by a two-dimensional perfectly conducting triangular cylinder is calculated using both the EEC's and the method of moments applied to the magnetic- and electric field integral equations (MFIE and EFIE, respectively). The consideration of a two-dimensional structure is convenient because it has no corners. The purpose of performing the numerical comparison is twofold. First, it is shown that the un-truncated EEC's are inadequate for bistatic analysis. Second, the singularity problems associated with Michaeli's expressions for the truncated EEC's are illustrated and it is shown that these singularities are not present in the new truncated EEC's derived in this report.

Both the FW field and the total scattered field are calculated. By considering the FW field it is possible to see how well the EEC's approximate the exact field in regions where the PO field is large compared to the FW field. The FW field is, however, not used without the PO field in practice. Therefore, the total scattered field is also calculated to illustrate a practical application of the EEC's.

5.1   The Fringe Wave Field

The lengths of the three sides of the triangular cylinder are all equal to 2λ, λ being the wavelength, and the illuminating field is a transverse electric (TE) polarized plane wave with direction of incidence shown in Figure 5.1. The FW field is calculated in the far field of the structure and expressed in terms of the two-dimensional radar cross section (RCS). The direction to the far field observation point is determined by the angle φ. To avoid the removable singularities in the EEC's, φ is assigned the values 0.1+n degrees, n being an integer ranging from 0 to 359. Figure 5.2 shows the FW field calculated from the difference between the MFIE solution and the PO solution, and from the un-truncated EEC's. It is seen that the un-truncated EEC's yield a poor approximation to the exact scattered FW field: The Ufimtsev singularity occurs for $\varphi=60$ degrees and the field is discontinuous across

the current layers located at φ=120, 180, 240, and 360 degrees. In addition, discontinuities at $\varphi = 60$ and $\varphi = 300$ degrees exist but these cannot be seen on the RCS plot of Figure 5.2. However, the phase of the scattered field reveals the discontinuities. Theoretically, the Ufimtsev singularity should only appear for grazing incidence. However, due to the finite numerical accuracy the singularity also appears for nearly grazing incidence, as in the configuration under consideration (see Figure 5.1).

Figures 5.3 and 5.4 show the results when the truncated EEC's are used. Figure 5.3 shows Michaeli's results and in Figure 5.4 the results obtained from the new truncated EEC's are shown. From both figures it is seen that the Ufimtsev singularity and the discontinuities across the current layers disappear. However, Figure 5.3 reveals that five spikes occur in the far field obtained from Michaeli's truncated EEC's when φ=61, 179, 299, 300, and 301 degrees. These spikes are caused by the non-removable singularities in Michaeli's expressions. The spikes at φ=61, 179, 299, and 301 degrees are caused by the singularity occurring when $\phi_0 = -(\alpha + \pi) + 2\pi N$ (see the discussion in Section 3.3) which is almost satisfied for edges B and C (see Figure 5.1). The spike at φ =300 occurs because α is close to π (see Section 3.3) for edge B. As noticed from Figure 5.4 no spikes occur when the new truncated EEC's are used. However, the agreement between the two methods of calculation is not perfect. This discrepancy occurs because the truncated EEC's only take into account part of the second-order edge diffraction, as explained at the end of Chapter 2, and for TE polarization the multiple interactions between the edges are significant.

Next, the incident plane wave is assumed to be transverse magnetic (TM) polarized (see Figure 5.5). Figures 5.6, 5.7, and 5.8 show the comparison among the results obtained from the difference between the EFIE solution and the PO solution, the un-truncated EEC's, and the truncated EEC's. For TM polarization the electric field has only a component parallel to the current layers and thus the field obtained from the un-truncated EEC's is not discontinuous across these layers. However, the derivative of the field with respect to φ is discontinuous. Figure 5.8 shows that the spikes encountered when Michaeli's truncated EEC's are applied (see Figure 5.7) are not present when the new truncated EEC's are used. Furthermore, almost perfect agreement between the two methods of calculation is observed in Figure 5.8. This is because the multiple interactions between the edges are weak for TM polarization.

In conclusion, the un-truncated EEC's are inadequate for analysis of bistatic scattering and the numerical comparison reveals that the new truncated EEC's, derived in this report, give a good approximation to the exact scattered FW field even when the distance between the edges is as small as 2λ.

23

5.2 The Total Scattered Field

First, the configuration shown in Figure 5.1, where the incident plane wave is TE polarized, is considered. Figure 5.9 shows the total scattered field calculated from the MFIE solution and from the sum of the solutions obtained using PO and the un-truncated EEC's. It is seen that the un-truncated EEC's yield a poor approximation to the exact scattered field. In Figure 5.10 the sum of the PO field and the field obtained from the new truncated EEC's is shown. The agreement with the MFIE solution is much better than that produced by the un-truncated EEC's. Moreover, the agreement between the results obtained using the new truncated EEC's and the MFIE solution is much better for the total scattered field than for the FW field alone shown in Figure 5.4.

Figures 5.11 and 5.12 show the total scattered field when the incident plane wave is TM polarized, as shown in Figure 5.5. In Figure 5.11 the un-truncated EEC's are used to approximate the FW part of the total scattered field and again a poor approximation to the exact field is obtained. However, when the new truncated EEC's are used, almost perfect agreement is achieved (see Figure 5.12).
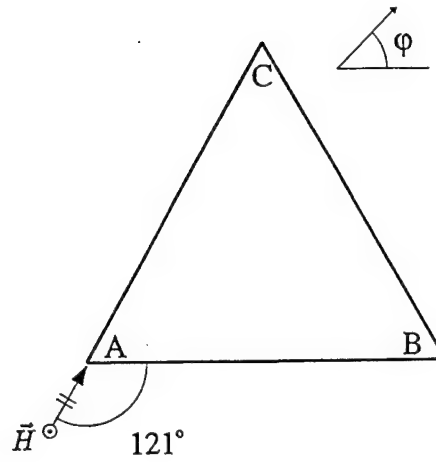
Figure 5.1: Cross-section of triangular cylinder with side length 2λ illuminated by a TE plane wave.
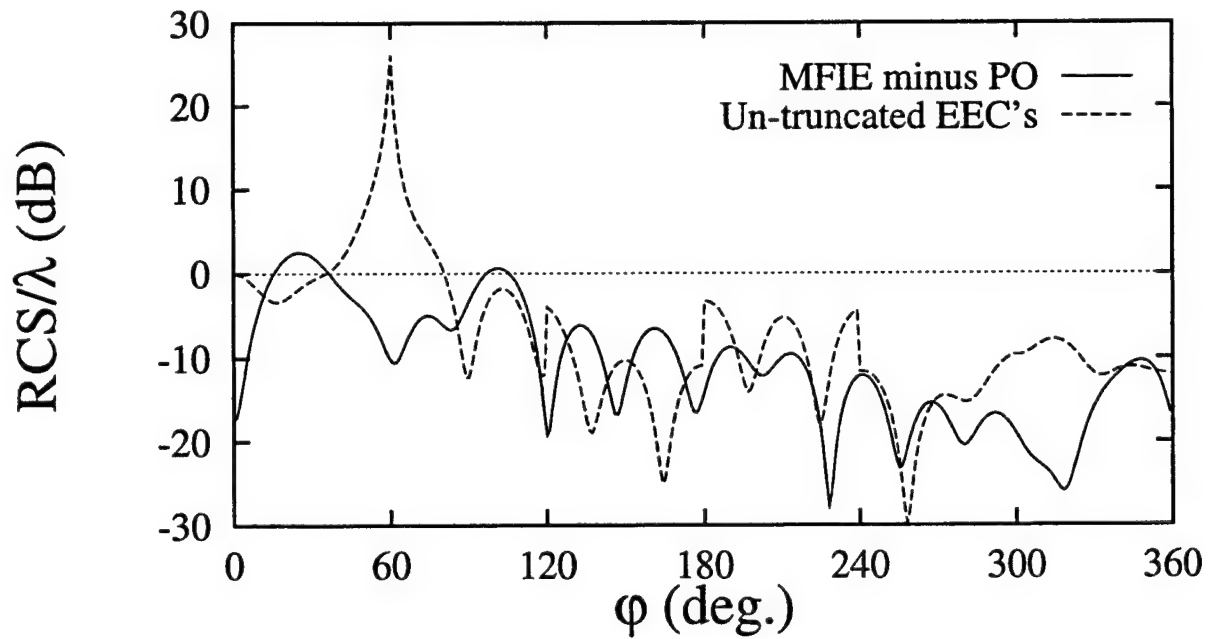

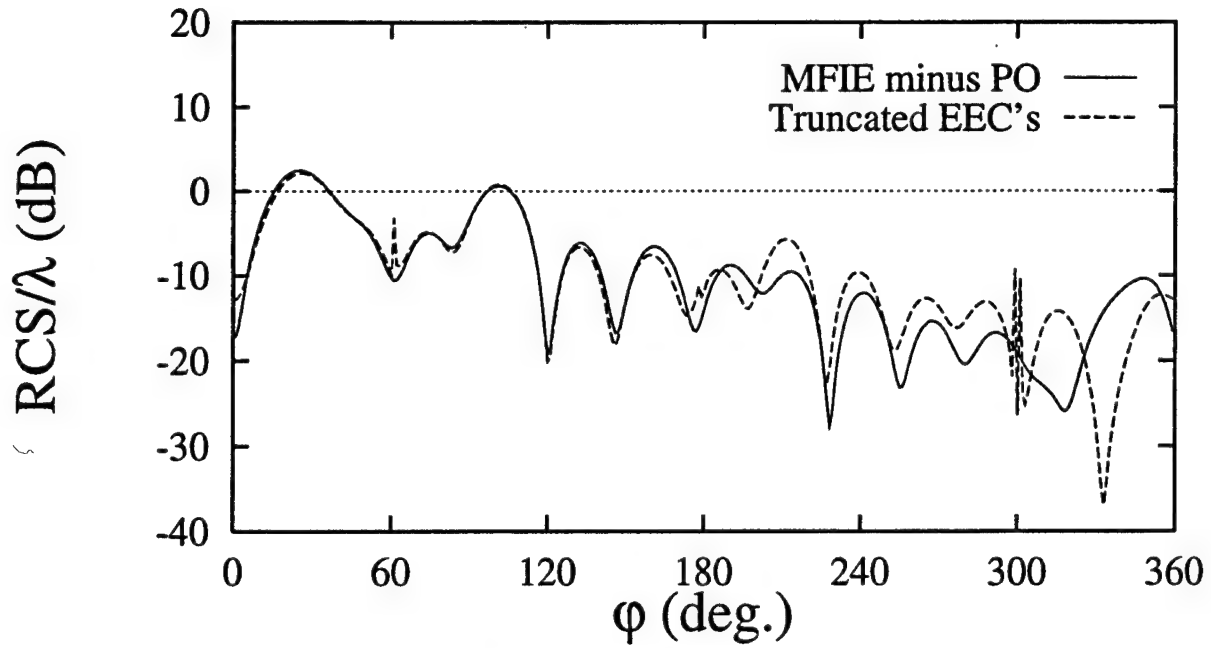Figure 5.2: FW field for the configuration shown in Figure 5.1.

Figure 5.3: FW field for the configuration shown in Figure 5.1. Michaeli's expressions are used to calculate the truncated EEC's.
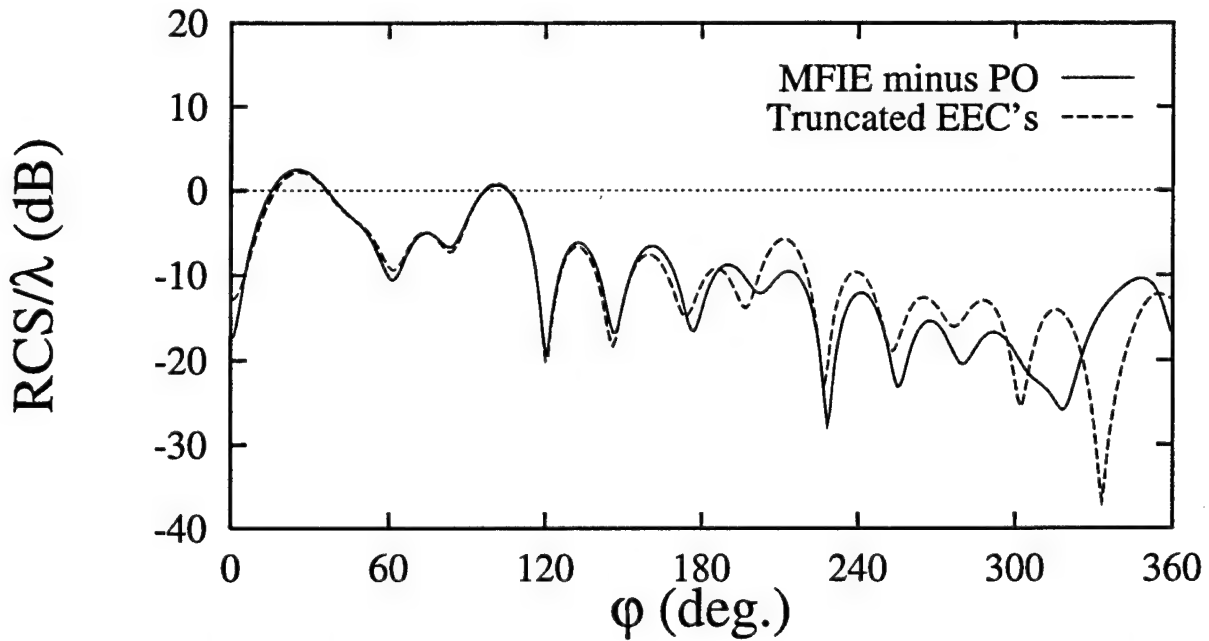

Figure 5.4: FW field for the configuration shown in Figure 5.1. The new truncated EEC's are employed.
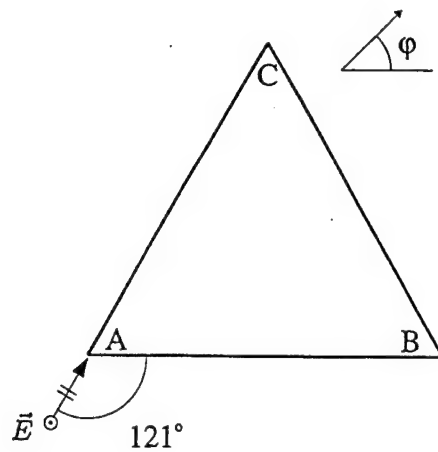
26

Figure 5.5: Cross-section of triangular cylinder with side length 2λ illuminated by a TM plane wave.
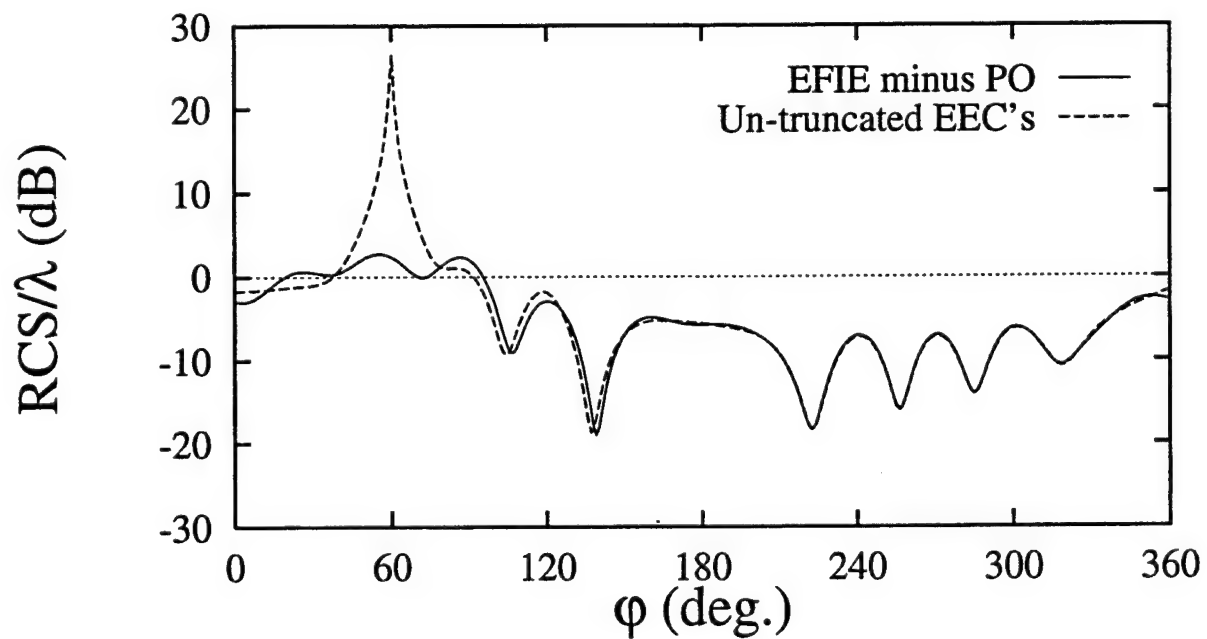

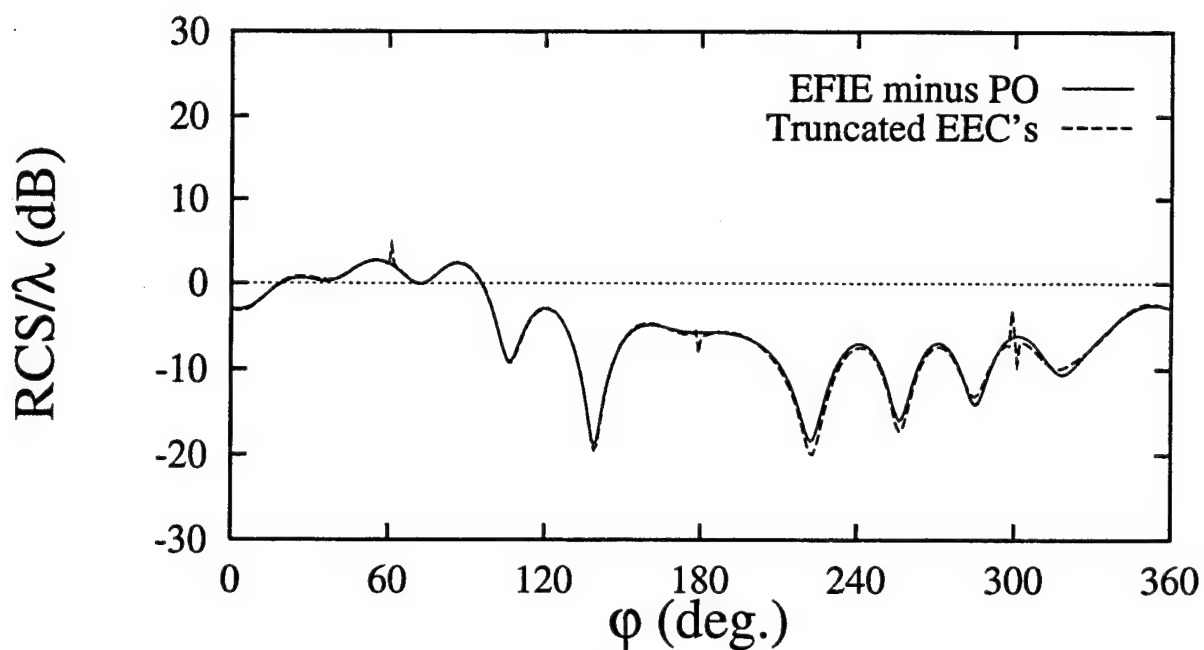Figure 5.6: FW field for the configuration shown in Figure 5.5.

Figure 5.7: FW field for the configuration shown in Figure 5.5. Michaeli's expressions are used to calculate the truncated EEC's.
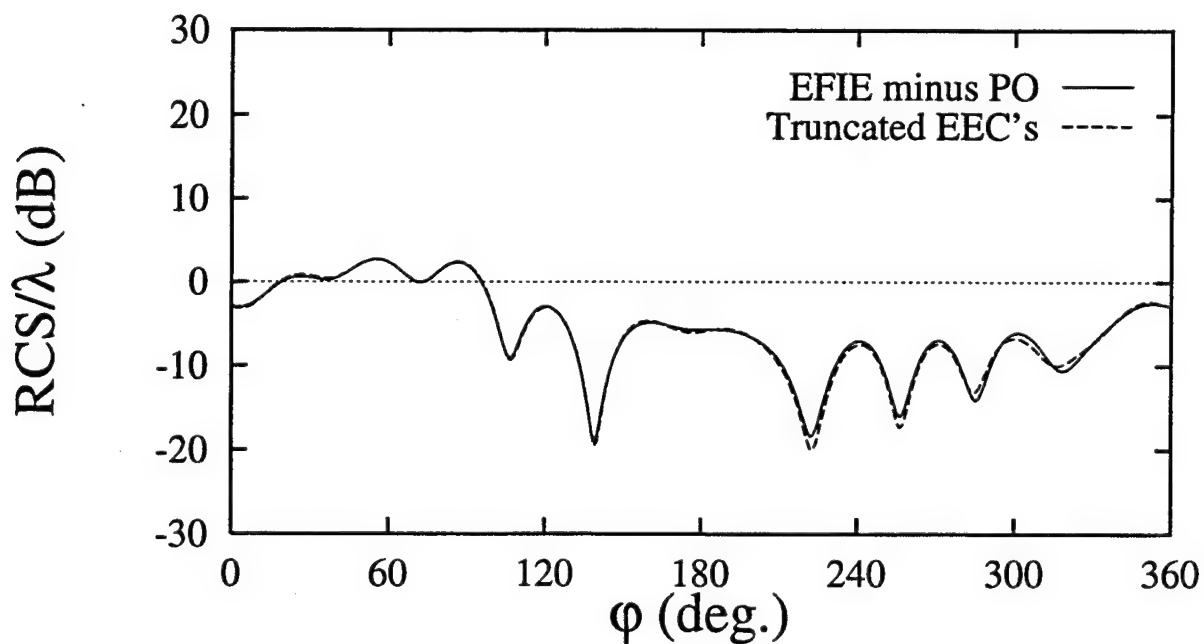

Figure 5.8: FW field for the configuration shown in Figure 5.5. The new truncated EEC's are employed.
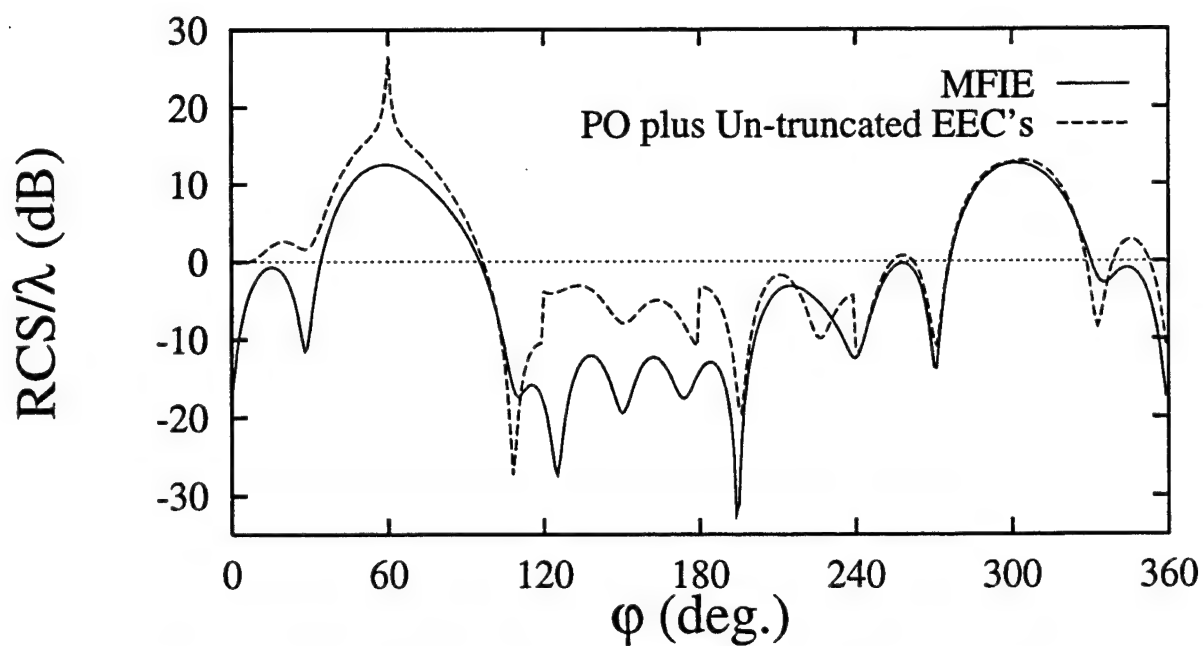
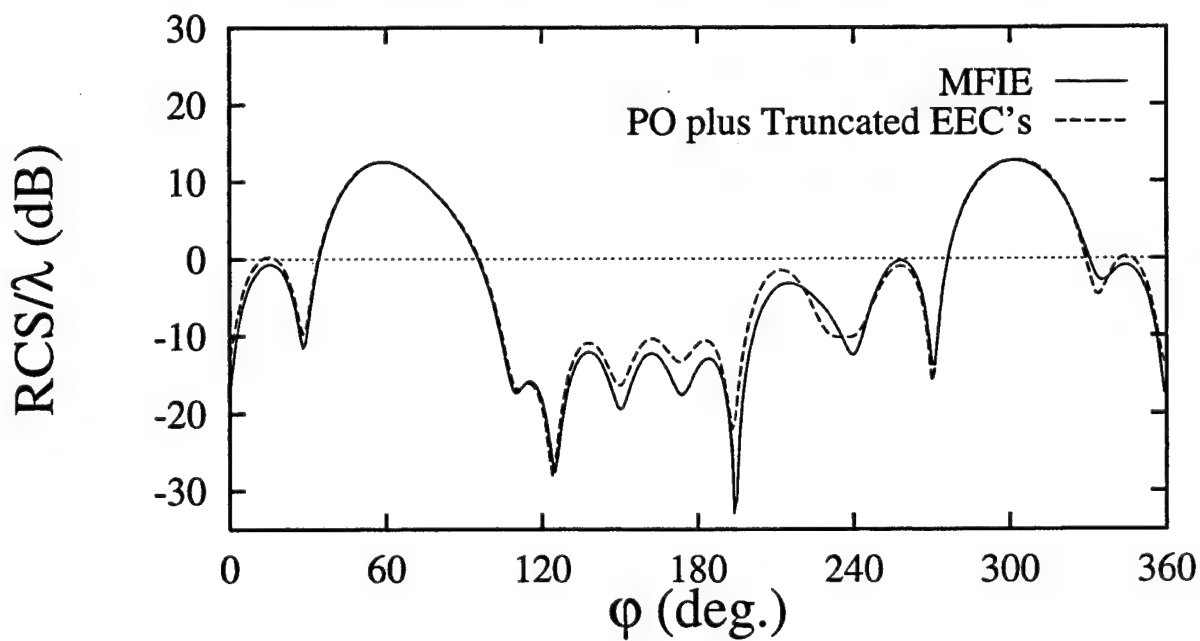Figure 5.9: Total scattered field for the configuration shown in Figure 5.1.

Figure 5.10: Total scattered field for the configuration shown in Figure 5.1. The new truncated EEC's are employed.
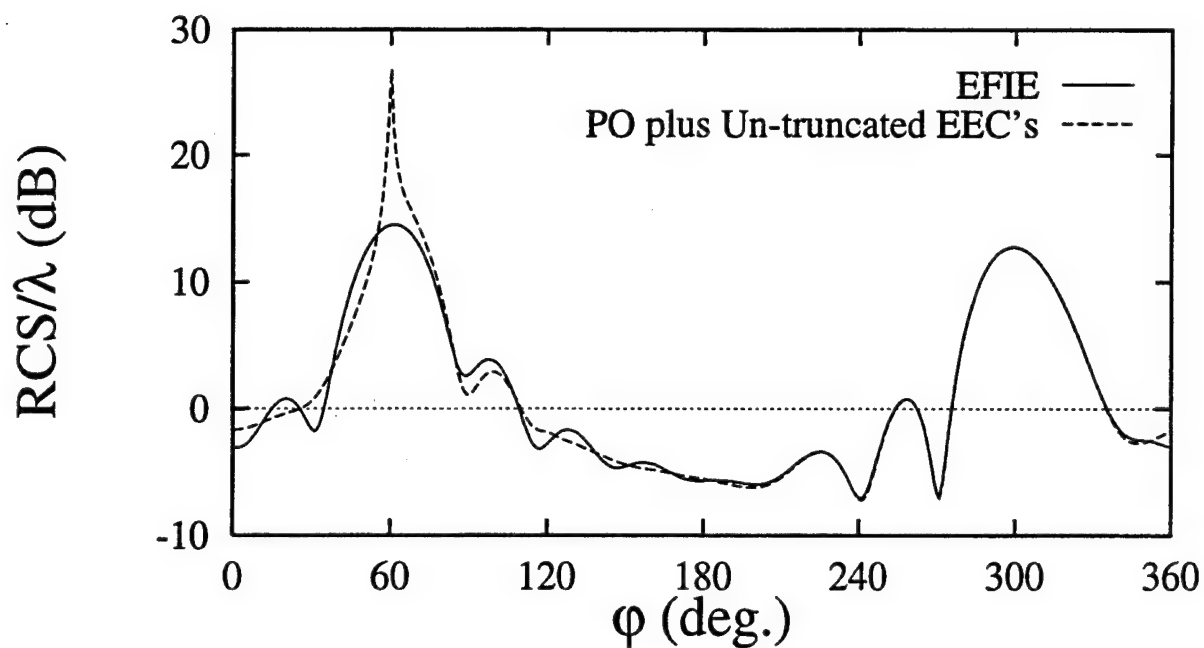
29

Figure 5.11: Total scattered field for the configuration shown in Figure 5.5.
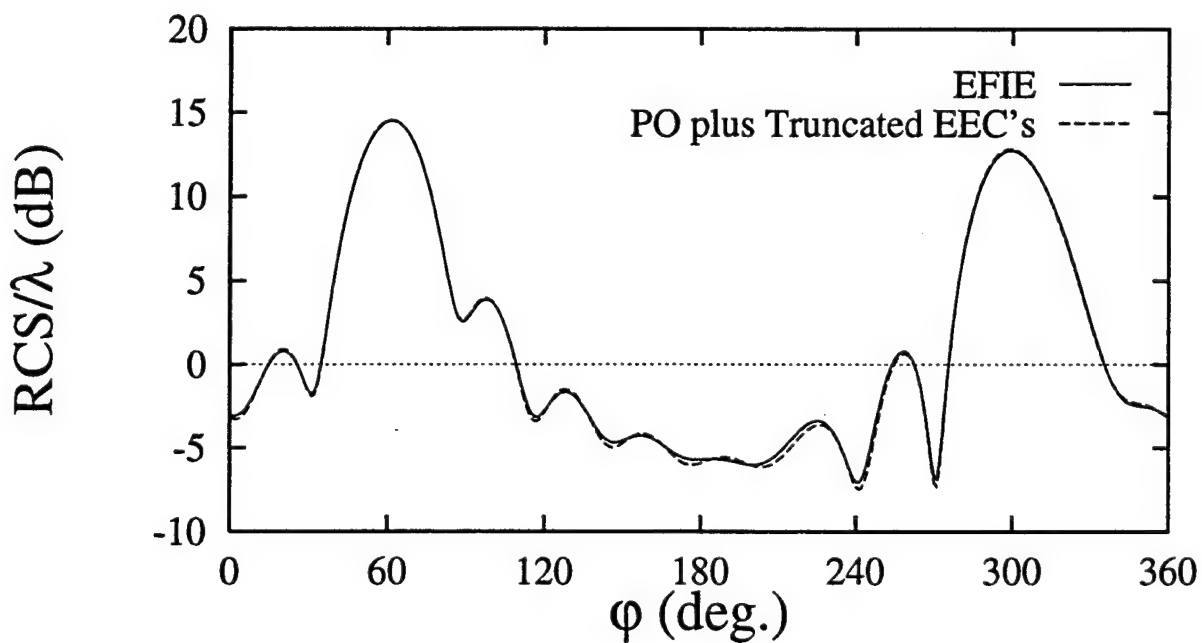

Figure 5.12: Total scattered field for the configuration shown in Figure 5.5. The new truncated EEC's are employed.

Chapter 6

Conclusions

New closed-form uniform expressions for physical theory of diffraction equivalent edge currents have been derived for truncated incremental wedge strips. The new truncated EEC's are well-behaved for all directions of incidence and observation. The expressions are asymptotic for $L \gg 1$, L being a parameter proportional to the strip length; however, they take a finite value when L is zero. This implies that the new truncated EEC's are well-suited for the analysis of bistatic radar scattering from perfectly conducting three-dimensional structures with plane faces.

Numerical results were presented showing that the use of truncated strips is necessary for the analysis of bistatic radar scattering. Furthermore, it was shown that the singularities occuring in the previously reported truncated EEC's are not present in the new truncated EEC's derived in this report.

References

[1] Michaeli, A. (1984) Equivalent edge currents for arbitrary aspects of observation, *IEEE Trans. Antennas Propagat.*, **32**, no. 3:252–258,
and (1985) Corrections to "Equivalent edge currents for arbitrary aspects of observation," *IEEE Trans. Antennas Propagat.*, **33**, no. 2:227.

[2] Michaeli, A. (1986) Elimination of infinities in equivalent edge currents, part I: Fringe current components, *IEEE Trans. Antennas Propagat.*, **34**, no. 7:912–918.

[3] Mitzner, K. M. (1974) *Incremental Length Diffraction Coefficients,* Technical Report AFAL-TR-73-296, Northrop Corporation.

[4] Shore, R. A. and Yaghjian, A. D. (1988) Incremental diffraction coefficients for planar surfaces, *IEEE Trans. Antennas Propagat.*, **36**, no. 1:55–70,
and (1989) Correction to "Incremental diffraction coefficients for planar surfaces," *IEEE Trans. Antennas Propagat.*, **37**, no. 10:1342.

[5] Breinbjerg, O. (1992) Higher order equivalent edge currents for fringe wave radar scattering by perfectly conducting polygonal plates, *IEEE Trans. Antennas Propagat.*, **40**, no. 12:1543–1554.

[6] Shore, R. A. and Yaghjian, A. D. (1992) Incremental diffraction coefficients for plane conformal strips with application to bistatic scattering from the disk, *Journal of Electromagnetic Waves and Applications*, **6**, no. 3:359–396.

[7] Cote, M. G., Woodworth, M. B., and Yaghjian, A. D. (1988) Scattering from the perfectly conducting cube, *IEEE Trans. Antennas Propagat.*, **36**, no. 9:1321–1329.

[8] Michaeli, A. (1987) Equivalent currents for second-order diffraction by the edges of perfectly conducting polygonal surfaces, *IEEE Trans. Antennas Propagat.*, **35**, no. 2:183–190.

[9] James, G. L. (1976) *Geometrical Theory of Diffraction for Electromagnetic Waves*, Peter Peregrinus Ltd.

[10] Bowman, J. J., Senior, T. B. A., and Uslenghi, P. L. E. (1969) *Electromagnetic and Acoustic Scattering by Simple Shapes*, North-Holland Publishing Company, p. 90.

[11] Felsen, L. B. and Marcuvitz, N. (1973) *Radiation and Scattering of Waves*, Prentice Hall, Englewood Cliffs, N. J., Chap. 4.

[12] Gennarelli, C. and Palumbo, L. (1984) A uniform asymptotic expansion of a typical diffraction integral with many coalescing simple pole singularities and a first-order saddle point, *IEEE Trans. Antennas Propagat.*, **32**, no. 10:1122–1124.

Appendix A

Asymptotic Expressions for I_2 and I_3

Using the same procedure that was used for the asymptotic calculation of I_1 in Section 4.1, I_2 is expressed as

$$I_2 = \sqrt{2j}\exp(-jX)\left(A_2\int_{-\infty}^{\infty}\frac{\exp(-Xs^2)}{s+\frac{a}{\sqrt{j}}}\,ds + \int_{-\infty}^{\infty}R_2(\xi)\exp(-Xs^2)\,ds\right) \tag{A.1}$$

with

$$A_2 = \lim_{\xi\to\phi_0}\frac{\sin\xi\sqrt{\frac{2}{j}}(-\cos\frac{\xi}{2}+\cos\frac{\phi_0}{2})}{\sin\frac{\xi}{2}(\cos\frac{\xi}{N}-\cos\frac{\phi_0}{N})} = \frac{-N\sin\phi_0}{\sqrt{2j}\sin\frac{\phi_0}{N}} \tag{A.2}$$

and

$$R_2(\xi) = \frac{\sin\xi}{(\cos\frac{\xi}{N}-\cos\frac{\phi_0}{N})\sin\frac{\xi}{2}} - \frac{A_2}{s+\frac{a}{\sqrt{j}}}. \tag{A.3}$$

The asymptotic result for $X\gg 1$ is

$$I_2 \sim \frac{-2jN\pi\sin\phi_0\exp(-jX)}{\sin\frac{\phi_0}{N}}\mathrm{sgn}(a)\left(F(|a|\sqrt{X}) - \frac{1}{2\sqrt{j\pi X}|a|}\right). \tag{A.4}$$

The expression for I_3 is

$$I_3 = \sqrt{2j}\exp(-jX)\left(A_3\int_{-\infty}^{\infty}\frac{\exp(-Xs^2)}{s+\frac{a}{\sqrt{j}}}\,ds + \int_{-\infty}^{\infty}R_3(\xi)\exp(-Xs^2)\,ds\right) \tag{A.5}$$

with

$$\begin{aligned}A_3 &= \lim_{\xi\to\phi_0}\frac{\cos\xi\sin\frac{\xi}{N}\sqrt{\frac{2}{j}}(-\cos\frac{\xi}{2}+\cos\frac{\phi_0}{2})}{\sin\frac{\xi}{2}(\cos\frac{\xi}{N}-\cos\frac{\phi_0}{N})}\\ &= \frac{-N\cos\phi_0}{\sqrt{2j}}\end{aligned} \tag{A.6}$$

and

$$R_3(\xi) = \frac{\cos\xi \sin\frac{\xi}{N}}{\cos\frac{\xi}{N} - \cos\frac{\phi_0}{N}} - \frac{A_3}{s + \frac{a}{\sqrt{j}}}. \tag{A.7}$$

The asymptotic evaluation of (A.5) yields

$$
\begin{aligned}
I_3 \quad \sim \quad & -2j\pi N \mathrm{sgn}(a) \cos\phi_0 \exp(-jX) F(|a|\sqrt{X}) \\
& + \exp(-jX)\sqrt{\frac{2j\pi}{X}} \left(\frac{N\cos\phi_0}{\sqrt{2}a} - \frac{\sin\frac{\pi}{N}}{\cos\frac{\pi}{N} - \cos\frac{\phi_0}{N}} \right).
\end{aligned} \tag{A.8}
$$

Appendix B

Evaluation of Integrals

In this appendix the integrals

$$F_1 = \int\limits_{l^A}^{\infty} \frac{\exp(-jku \sin^2 \beta_0 (1 - \mu))}{\sqrt{u}} \, du \tag{B.1}$$

and

$$F_2 = \int\limits_{l^A}^{\infty} F(\sqrt{2ku} \sin \beta_0 | \cos \frac{\phi_0}{2} |) \exp(-jku \sin^2 \beta_0 (1 - \mu)) \, du \tag{B.2}$$

are calculated. It is noted that $\mu \leq 1$. Thus, applying the substitution $t^2 = uk \sin^2 \beta_0 (1 - \mu)$ and assuming that $\sin^2 \beta_0 (1 - \mu) \neq 0$, the integral F_1 becomes

$$F_1 = \frac{2}{\sqrt{k(1 - \mu)} \sin \beta_0} \int\limits_{\sqrt{L(1-\mu)}}^{\infty} \exp(-jt^2) \, dt \tag{B.3}$$

which is expressed in terms of the modified Fresnel function F (3.22)

$$F_1 = \frac{2\sqrt{\pi} \exp(jL(\mu - 1))}{\sqrt{jk(1 - \mu)} \sin \beta_0} F(\sqrt{L(1 - \mu)}) \tag{B.4}$$

where $L = kl^A \sin^2 \beta_0$. For $\sin^2 \beta_0 (1 - \mu) = 0$ the integral F_1 is singular.

The integral F_2 can be rewritten as

$$F_2 = \sqrt{\frac{j}{\pi}} \int\limits_{l^A}^{\infty} \exp(jku \sin^2 \beta_0 (\mu + \cos \phi_0)) \int\limits_{\sqrt{2ku} \sin \beta_0 | \cos \frac{\phi_0}{2} |}^{\infty} \exp(-jt^2) \, dt \, du \tag{B.5}$$

37

which for $\sin^2 \beta_0 (\mu + \cos \phi_0) \neq 0$ is evaluated using integration by parts

$$F_2 = \sqrt{\frac{j}{\pi}} \left[\frac{\exp(jku \sin^2 \beta_0(\mu + \cos \phi_0))}{jk \sin^2 \beta_0(\mu + \cos \phi_0)} \int\limits_{\sqrt{2ku} \sin \beta_0 |\cos \frac{\phi_0}{2}|}^{\infty} \exp(-jt^2)\, dt \right]_{lA}^{\infty}$$

$$+ \sqrt{\frac{j}{\pi}} \int\limits_{lA}^{\infty} \frac{\exp(jku \sin^2 \beta_0(\mu + \cos \phi_0))}{jk \sin^2 \beta_0(\mu + \cos \phi_0)} \exp(-2jku \sin^2 \beta_0 \cos^2 \frac{\phi_0}{2})$$

$$\cdot \frac{\sqrt{k} \sin \beta_0 |\cos \frac{\phi_0}{2}|}{\sqrt{2u}}\, du$$

$$= \frac{-\exp(jL(\mu + \cos \phi_0))}{\sqrt{j\pi} k \sin^2 \beta_0(\mu + \cos \phi_0)} \int\limits_{\sqrt{2L}|\cos \frac{\phi_0}{2}|}^{\infty} \exp(-jt^2)\, dt$$

$$+ \frac{|\cos \frac{\phi_0}{2}|}{\sqrt{2j\pi k} \sin \beta_0(\mu + \cos \phi_0)} F_1. \tag{B.6}$$

Using the expression for F_1 in (B.4), the result

$$F_2 = \frac{\exp(jL(\mu - 1))}{jk \sin^2 \beta_0(\mu + \cos \phi_0)} \left(-F(\sqrt{2L}|\cos \frac{\phi_0}{2}|) + \frac{\sqrt{2}|\cos \frac{\phi_0}{2}|}{\sqrt{1 - \mu}} F(\sqrt{L(1 - \mu)}) \right) \tag{B.7}$$

is obtained. This expression has a finite limit for $\sin^2 \beta_0(\mu + \cos \phi_0) \rightarrow 0$.

MISSION

OF

ROME LABORATORY

Mission. The mission of Rome Laboratory is to advance the science and technologies of command, control, communications and intelligence and to transition them into systems to meet customer needs. To achieve this, Rome Lab:

a. Conducts vigorous research, development and test programs in all applicable technologies;

b. Transitions technology to current and future systems to improve operational capability, readiness, and supportability;

c. Provides a full range of technical support to Air Force Materiel Command product centers and other Air Force organizations;

d. Promotes transfer of technology to the private sector;

e. Maintains leading edge technological expertise in the areas of surveillance, communications, command and control, intelligence, reliability science, electro-magnetic technology, photonics, signal processing, and computational science.

The thrust areas of technical competence include: Surveillance, Communications, Command and Control, Intelligence, Signal Processing, Computer Science and Technology, Electromagnetic Technology, Photonics and Reliability Sciences.